High quality graphene oxide–CdS–Pt nanocomposites for efficient photocatalytic hydrogen evolution

Gao, Peng; Liu, Jincheng; Lee, Siew Siang; Zhang, Tong; Sun, Darren Delai

2011

Gao, P., Liu, J., Lee, S., Zhang, T., & Sun, D. D. (2011). High quality graphene oxide-CdS-Pt nanocomposites for efficient photocatalytic hydrogen evolution. Journal of Materials Chemistry, 22, 2292-2298.

https://hdl.handle.net/10356/100812

https://doi.org/10.1039/c2jm15624e

Journal Name

Dynamic Article Links ►

Cite this: DOI: 10.1039/c0xx00000x

www.rsc.org/xxxxxx

ARTICLE TYPE

High quality Graphene Oxide-CdS-Pt nanocomposites for efficient photocatalytic hydrogen evolution

Peng Gao, Jincheng Liu,* Siewsiang Lee, Tong Zhang, and Darren Delai Sun*

Received (in XXX, XXX) Xth XXXXXXXXX 20XX, Accepted Xth XXXXXXXXX 20XX

DOI: 10.1039/b000000x

Graphene Oxide-CdS-Pt (GO-CdS-Pt) nanocomposites with different amounts of Pt nanoparticles were successfully synthesized *via* the formic acid reduction process followed by a two-phase mixing. The morphology, crystal phase and optical properties of obtained composites were well characterized by atomic force microscopy (AFM), transmission electron microscopy (TEM), X-ray diffraction (XRD), UV-vis spectroscopy, Fourier transform IR spectroscopy (FT-IR) and X-ray photoelectron spectroscopy (XPS), respectively. The photocatalytic activity of GO-CdS-Pt composites for hydrogen generation was investigated. The results show that the GO-CdS-Pt composite containing 0.5 at% of Pt exhibits the highest hydrogen evolution rate of 123 mL $h^{-1}g^{-1}$ with strong photostability, which is about 2.5 times higher than that of GO-CdS, and 10.3 times higher than that of CdS. The increased photocatalytic hydrogen generation efficiency is attributed to the effective charge separation and decreased anti-recombination with the addition of GO and Pt, as well as the low over potential of Pt for water splitting. Our findings pave a way to design multi-component graphene-based composites for highly efficient H_2 generation and other applications.

Introduction

For the past centuries, fossil fuels such as petroleum, coal and natural gas have been consumed excessively in pursuing for rapid economic growth.[1] Due to global warming and climate change caused by the consumption of fossil fuels, there is an urgent need for us to find new ways to maintain our future energy supply 'sustainable', which not only keeps the economic growing but also protects the environment.[1-3] Hydrogen, which is considered as a new energy source is able to overcome the disadvantages of using conventional fossil fuels as it has high heat conversion efficiency, zero carbon emission, which gives us hopes as a potential renewable alternative energy in alleviating the enormous pressure on traditional fossil fuels for the future.[4, 5] Since the first report on photocatalytic water splitting via using TiO_2 photoelectrodes by Honda and Fujishima was published in 1972,[6] photocatalytic generation of hydrogen from water has received large research attentions during the past decades.

To date, many semiconductors, including TiO_2,[7] CdS,[8] $SrTiO_3$,[5] WO_3,[9] CuO[10] and so on，[11, 12] have been reported having the ability to generate hydrogen. Among them, CdS has been extensively studied due to (1) a relatively narrow band gap (ca. 2.4 eV), making it effective in absorbing incident light;[13] (2) the reduction and oxidation potential of water lie within the band gap of CdS – the conduction band (CB) of CdS (ca. -0.9 eV) is more negative than the reduction potential of H^+/H_2 (0 eV) while the valence band (VB) of CdS (ca. 1.5 eV) is more positive than the oxidation potential of O_2/H_2O (1.23 eV).[14] These two factors meet the requirements for effective hydrogen evolution. However, there are some bottlenecks, which limit the efficiency of hydrogen evolution by using pure CdS, including (1) rapid recombination rate of photogenerated electron-hole pairs leads to poor photocatalytic activity;[5, 15] (2)easy aggregation of CdS nanoparticles reduces the specific surface area and reactive sites;[15] (3) removing virulent CdS nanoparticles from water still remains a challenge.

Many attempts have been adopted to solve these drawbacks, such as solid-phase synthesis of uniform dispersed CdS nanostructure,[8] coupling CdS with other wide band gap semiconductors, especially TiO_2,[16] photodeposition of metals,[17] and combining CdS nanoparticles with graphene oxides (GO).[15, 18, 19] Among them, preparing GO based CdS composites has been demonstrated to be a promising method to overcome these bottlenecks, since GO is a chemically modified graphene, which posses immense specific surface area (theoretically 2600 m^2/g),[20] chemical stability and high water solubility.[21, 22] Li *et al.*[15] reported that CdS cluster decorated graphene nanosheets exhibited higher hydrogen evolution rate than pure CdS nanoparticles. Jia *et al.*[19] prepared N-doped graphene/CdS nanocomposites successfully and high hydrogen evolution rate was achieved. Although both of their work investigated the influence of graphene/CdS ratio on the hydrogen evolution ability, the effects of co-catalyst, such as platinum (Pt), were seldom mentioned. According to our knowledge, Pt plays a significant role in hydrogen evolution process, especially when it is combined with carbon based composites.[23] Hence, it is crucial to synthesize GO-CdS-Pt nanocomposites with uniform distribution of CdS and Pt nanoparticles on GO to achieve high hydrogen production rate as well as investigate the influence of Pt on

hydrogen evolution process.

In this work, GO-CdS-Pt nanocomposites with different amounts of Pt were successfully prepared via a combination of reduction process and the two-phase method.[24] This novel nanocomposite conquers the traditional problems of CdS and combines the advantages of respective component, leading to more benefits than previous CdS based photocatalysts, including (1) suppressing recombination of photogenerated electron-hole pairs to prolong the lifetime of charge carriers through effective charge transfer route from CdS→GO→Pt; (2) uniform deposition of CdS and Pt nanoparticles on GO without aggregation to maximize the specific surface area; and (3) easy removal of this nanocomposite from aqueous solution via centrifugation. Herein, GO-CdS-Pt nanocomposites were synthesized successfully and highly efficient photocatalytic hydrogen evolution rate was achieved. In addition, influence of Pt and hypothetic mechanism of hydrogen evolution process are presented here. This novel nanocomposite shows great potential in commercial energy production.

Experimental

Synthesis of Graphene oxide (GO)

GO was synthesized by the modified Hummers' method.[25, 26] In a typical procedure, 500 mg of graphite powder and 2.0 g of sodium nitrate ($NaNO_3$) were put into cold (below 5 °C) concentrated H_2SO_4 (18 mL, 98%). This mixture was stirred continuously for 1 h and the temperature was kept below 5 °C by cooling in an ice bath. Then, 3 g of potassium permanganate ($KMnO_4$) was added gradually and reaction was continued for another 2 h at temperature below 5 °C. The mixture was then heated to 35 °C for 30 min, and then 40 mL of deionized (DI) water was added slowly while the temperature was increased and kept at 100 °C for 15 min. The mixture was diluted with 70 mL of DI water when it cooled to room temperature. The color of suspension changed to bright yellow after adding 10 mL of H_2O_2 (35%). For thorough purification, the suspension was filtered and washed with 400 mL of 5% HCl twice followed by further washing with 200 mL of DI water for 3 times. Finally, the as-obtained precipitate was dried in the vacuum drier for at least 5 days for further use.

Synthesis of CdS nanoparticles

The spherical-shaped CdS nanopartcles were synthesized by the method described in previous report.[27] In a typical procedure, 604 mg of cadmium chloride-1-hydrate ($CdCl_2 \cdot H_2O$) (3 mmol) was well dissolved in 30 mL of oleylamine. Then, the mixture was transferred to a three-necked flask and was heated to 90 °C for 1 h. Thereafter, 48 mg of sulfur (S) (1.5 mmol) well dissolved in 5 mL of oleylamine was injected to the system and the mixture was heated to 160 °C with vigorous stirring and nitrogen protecting for another 6 h. Finally, the resulting CdS nanoparticles were retrieved by adding acetone followed by centrifugation.

Synthesis of GO-Pt

Typically, 50 mg of as prepared GO was dissolved in 50 mL of DI water and sonicated for 30 min. Different amounts (5 mg, 8 mg and 10 mg) of hexachloroplatinic acid ($H_2PtCl_6 \cdot 6H_2O$) were dissolved in 10 mL of DI water, individually, and then mixed with GO solution. Then, the pH of the mixture was adjusted to 7 using diluted sodium hydroxide (NaOH). Thereafter, the mixture was transferred to a three-necked flask and was then heated to 80 °C under nitrogen flow. 1 mL of formic acid (HCOOH) was then injected into the solution, and the reaction continued for 15 min at 80 °C. The product was centrifuged and washed with DI water for several times.

Synthesis of GO-CdS and GO-CdS-Pt

GO-CdS and GO-CdS-Pt were synthesized by two-phase method described by our previous reports.[24, 28] In a typical synthesis, 50 mg of as synthesized GO or GO-Pt was well dissolved in 20 mL of DI water. 15 mg of as prepared CdS was dispersed in 20 mL of toluene and was added to GO or GO-Pt solution. The mixture was kept stirring for 24 h and followed by washing with acetone and tetrahydrofuran. The final obtained GO-CdS-Pt composites were labeled as GCP-1, GCP-2 and GCP-3 in accordance with different amounts of Pt (5 mg, 8mg and 10 mg), respectively.

Characterization and hydrogen evolution

Surface topography of GO sheets was characterized by atomic force microscopy (AFM). The morphology of as prepared GO, GO-Pt, GO-CdS and GO-CdS-Pt were evaluated by transmission electron microscopy (TEM, JEOL 2010-H) operating at 200 kV. The structure and crystal phase of GO-Pt, GO-CdS and GO-CdS-Pt composites were examined by X-ray diffraction (XRD, Shimadzu XRD-6000) with monochromated high-intensity Cu Kα radiation (λ=1.5418 Å) operated at 40 kV and 30 mA. Ultraviolet-visible spectrometer (3000 UV-visible) was adopted to identify the absorption edges of CdS, GO-Pt, GO-CdS and GO-CdS-Pt. X-ray photoelectron spectroscopy (XPS) measurements were done by using a Kratos Axis Ultra Spectrometer with a monochromic Al Kα source at 1486.7 eV, with a voltage of 15 kV and an emission current of 10 mA. Furthermore, the binding energy (BE) values were calibrated by using carbonaceous C 1s line (284.8 eV) as a reference. FT-IR spectra were recorded on a Perkin Elmer GX FT-IR system by using compressed KBr disc technique. A Dilor LABRAM-1B microspectrometer with 532 nm laser excitation was used to record the Raman spectra of GO, GO-CdS, GO-Pt and GO-CdS-Pt.

The photocatalytic hydrogen evolution reaction was performed in an inner-irradiation type Pyrex reactor (volume: 270 ml) with a 400 W high pressure Hg lamp (Riko, UVL-400HA) as the light source, the peak wavelength of which is centered at 365 nm. To maintain a constant reactor temperature of 25 °C, a quartz water jacket, which was cooled by recycled water, was utilized to cover the lamp. 50 mg of powdered photocatalyst was suspended in 10 volume% methanol water mixture. A magnetic stirrer was placed at the bottom of the reactor to ensure homogeneity of the suspension during reaction. Prior to irradiation, the photocatalyst suspension was de-aerated thoroughly for 30 min by nitrogen gas purging. Gas produced via the photocatalytic reaction was analyzed using an off-line TCD-type gas chromatography (Agilent 7890A, HP-PLOT MoleSieve/5A).

Results and discussion

Characterization of GO-CdS-Pt composites

AFM is employed to characterize the well synthesized GO sheets. In Fig. S1†, the single layer and some overlapping of GO sheets are clearly shown. The typical size of GO sheets is more than 2 μm, including some small ones. In addition, the thickness of GO sheets is measured around 1 nm through two line scans, which is slight larger than the reported thickness about 0.8 nm.[15, 29] This can be attributed to large amounts of oxygen-containing functional groups attached on both sides of GO sheets.

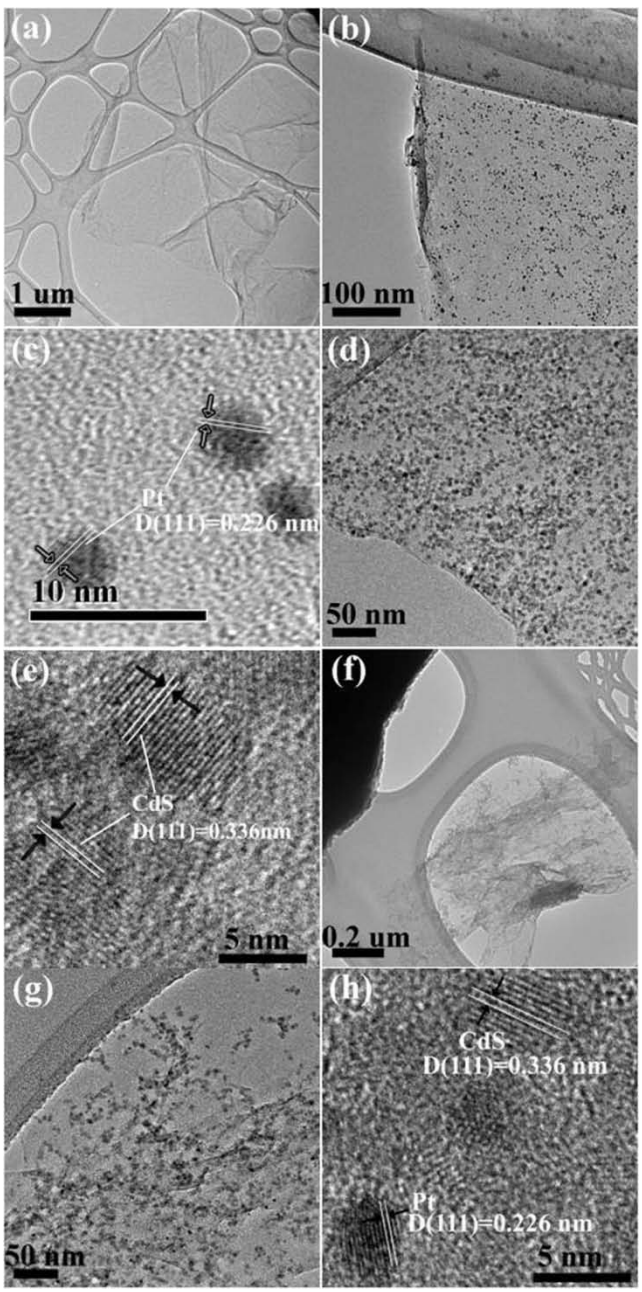

Fig. 1 TEM and HRTEM images of GO (a), GO-Pt (b-c), GO-CdS (d-e) and GCP-1 (f-h).

The morphologies and microstructures of the obtained products are analyzed with TEM. Fig. 1 shows the TEM images of GO (a), GO-Pt (b-c), GO-CdS (d-e) and GCP-3 (f-h), respectively. In Fig. 1 (a), the single layer GO sheet with characterized wrinkles and the size of more than 2 μm can be clearly observed, which further confirms the results of AFM image. The large GO sheets benefit the recovery of our products to eliminate environmental concerns. Fig. 1 (b) and (c) show the morphology of GO-Pt. Pt nanoparticles are uniformly deposited on GO sheets without aggregation, and some vacancies unoccupied by Pt will leave for CdS nanocrystals to attach (Fig. 1 (b)). Particularly, the synthesis process of GO-Pt is pivotal since if Pt nanoparticles take over all active sites of GO sheets, CdS nanocrystals cannot be anchored on GO. Fig. 1 (c) exhibits the high-resolution transmission electron microscopy (HRTEM) image of GO-Pt, in which the size of Pt nanoparticles is around 3 to 4 nm. The clear lattice-fringe spacing of individual Pt nanoparticle is 0.226 nm, assigning to the (111) crystal plane of face-centered cubic Pt.[30] In addition, the TEM image of GO-CdS (Fig. 1 (d)) shows that many CdS nanoparticles are well dispersed on GO sheets with uniform size around 5 to 6 nm. The HR-TEM image (Fig. 1 (e)) of GO-CdS shows the clear lattice of cubic CdS with spacing of 0.336 nm corresponding to the (111) facet,[15] indicating the high crystallinity of as-synthesized CdS nanocrystals. Furthermore, Fig. 1 (f), (g) and (h) show the morphology of GCP-3 nanocomposite. As shown in Fig. 1 (f), CdS and Pt nanoparticles are deposited on a whole GO sheet, and the size of this GO sheet is also larger than 2 μm, indicating that the GO sheets synthesized in our experiments typically have a large size. In Fig. 1 (g), the single and double layer of GO sheets are entirely covered by CdS and Pt nanoparticles, indicating that the methods adopted to produce GCP-3 nanocomposites are absolutely efficient, which can be further extended to synthesize other GO based composites. In addition, the effective deposition of CdS and Pt nanoparticles on GO sheets contributes to the effective hydrogen evolution due to high light harvesting ability and efficient charge transfer. Fig. 1 (h) exhibits perfectly crystallized nanoparticles of CdS and Pt with lattice spacing of 0.336 nm and 0.226 nm, which correspond to the (111) and (111) crystal planes of CdS and Pt, respectively. The particle sizes of CdS and Pt in GCP-3 nanocomposites are similar to that in sample of GO-CdS and GO-Pt. Fig. S2† shows additional TEM and HRTEM images of GCP-1 and GCP-2. The TEM analysis provides strong evidence that GO-Pt, GO-CdS and GO-CdS-Pt based on large GO sheets have been successfully synthesized.

XRD was used to determine the crystalline phases of as-synthesized samples. Fig. 2 (a) shows the XRD patterns of GO-Pt, GO-CdS and GO-CdS-Pt, respectively. As shown in Fig. 2 (a), the diffraction peaks at 2θ of 26.5, 44.0 and 52.1° are attributed to (111), (220) and (311) facets of cubic CdS (JCPDF 80-0019), respectively. In addition, diffraction peaks at 39.9, 46.3 and 67.7° correspond to (111), (200) and (220) diffraction planes of cubic Pt (JCPDF 70-2431), individually. No diffraction peaks of GO are observed because the regular stack of GO is destroyed by the intercalation of CdS and Pt nanoparticles.[24] These results indicate that CdS and Pt nanoparticles are successfully deposited on GO sheets. According to Scherrer's equation [16] [$D=0.9\lambda / \beta\cos\theta$, where D is the crystal size, λ is the wavelength of the X-ray radiation (0.15418 nm for Cu Kα), β is full width half maximum of the diffraction peak measured at 2θ and θ is the diffraction

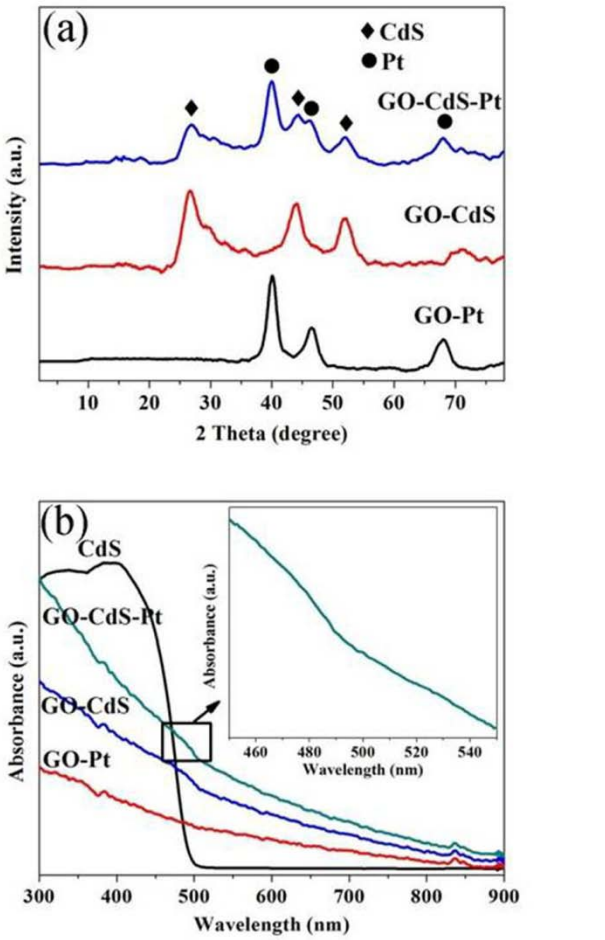

Fig. 2 XRD patterns of GO-Pt, GO-CdS and GO-CdS-Pt (a); and UV-vis absorption spectra of CdS, GO-Pt, GO-CdS and GO-CdS-Pt (b).

angle], the average particle size of CdS and Pt are estimated to be 5.1 nm and 3.6 nm corresponding to (111) and (111) reflections of CdS and Pt, respectively, which is consistent with the TEM analysis.

Fig. 2 (b) exhibits UV-vis absorption spectra of CdS, GO-Pt, GO-CdS and GO-CdS-Pt, individually. Pure CdS nanoparticles display a steep absorption in visible-light range, indicating the narrow size distribution of CdS nanocrystals with average diameter of 5.1 nm according to Peng's equation.[31] Meanwhile, GO-Pt shows no absorption onset in the wavelength range from 300 to 900 nm, indicating that it has no light absorption ability. However, GO-CdS and GO-CdS-Pt show similar weaker and broader absorption compared to pure CdS nanoparticles. In addition, the absorption edges of GO-CdS and GO-CdS-Pt are slightly red-shifted and continuous absorption bands from 500 to 900 nm are clearly exhibited in Fig. 2 (b) and inset, which contribute to the more effective activity of GO-CdS and GO-CdS-Pt than pure CdS nanocrystals. The differences of UV-vis spectra between GO-CdS, GO-CdS-Pt and pure CdS can be attributed to the introduction of GO sheets, the carbon species of which can absorb light and modify the surface of CdS nanoparticles.[19]

Fig. 3 shows the FT-IR spectra of GO, GO-CdS, GO-Pt and

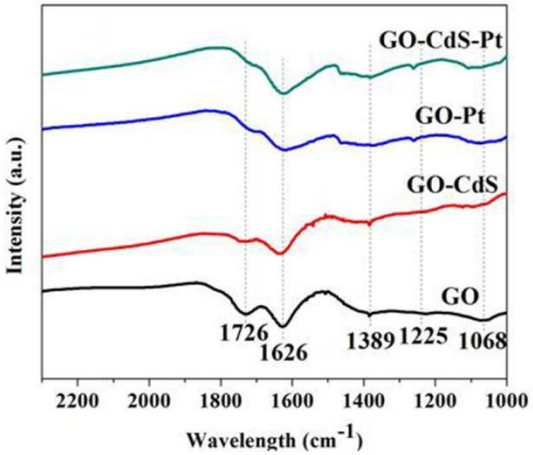

Fig. 3 FT-IR spectra of GO, GO-CdS, GO-Pt and GO-CdS-Pt.

GO-CdS-Pt, respectively. The hydrophilic groups of GO sheets are clearly displayed, including 1068 cm^{-1} (C-O stretching vibrations), 1225 cm^{-1} (phenolic C-OH stretching), 1389 cm^{-1} (carboxyl C-OH stretching), and 1726 cm^{-1} (C=O stretching vibrations of carboxyl), which are all attributed to carboxyl and phenolic groups of GO sheets, indicating that graphite is successfully oxidized into hydrophilic GO sheets.[18, 32] The hydrophilic GO sheets can be easily dissolved in water, which is beneficial to hydrogen generation process.[15] In addition, the peak at 1626 cm^{-1} can be assigned to H-O-H bending band of the adsorbed H_2O or the skeletal vibrations of unoxidized graphitic domains.[32, 33] FT-IR spectrum of GO-CdS shows similar peaks. However, although FT-IR spectra of GO-Pt and GO-CdS-Pt show similar peaks of carboxyl functional groups including (1068 cm^{-1}, 1389 cm^{-1} and 1726 cm^{-1}), the intensity of these peaks is reduced dramatically due to partial reduction of GO by formic acid during the synthesis of GO-Pt. As a consequence, the conductivity of GO-CdS-Pt is improved, which contributes to effective charge separation and anti-recombination of photogenerated electron-hole pairs during hydrogen evolution process.[24] Another difference between GO and GO-CdS, GO-Pt, GO-CdS-Pt FT-IR spectra is the slight shift of phenolic peak from 1225 cm^{-1} to higher wavelength around 1240 cm^{-1}. The reason for this shift has not been totally understood. The possible explanation is the interaction between CdS, Pt nanoparticles and GO sheets.

XPS is used to determine the quantity of elements, including C, O, Cd, S and Pt individually. Fig. 4 (a) exhibits the full XPS spectra of GO, GCP-1, GCP-2 and GCP-3, respectively. It is clearly shown that all of GO-CdS-Pt nanocomposites are comprised of C, O, Cd, S and Pt without any impurities. The atomic percentage of each element is analyzed by CasaXPS software according to the major peaks, including C 1s, O 1s, Cd 3d, S 2p and Pt 4f, as shown in the inset of Fig. 4 (a). The atomic percentages of CdS in all of these composites are around 1.8%, since the amount of CdS nanoparticles used during the experiments is the same. However, the atomic percentage of Pt for each GO-CdS-Pt nanocomposite is 0.35% for GCP-1, 0.45% for GCP-2 and 0.5% for GCP-3, respectively. The amount of Pt plays a significant role in generating H_2, which will be discussed

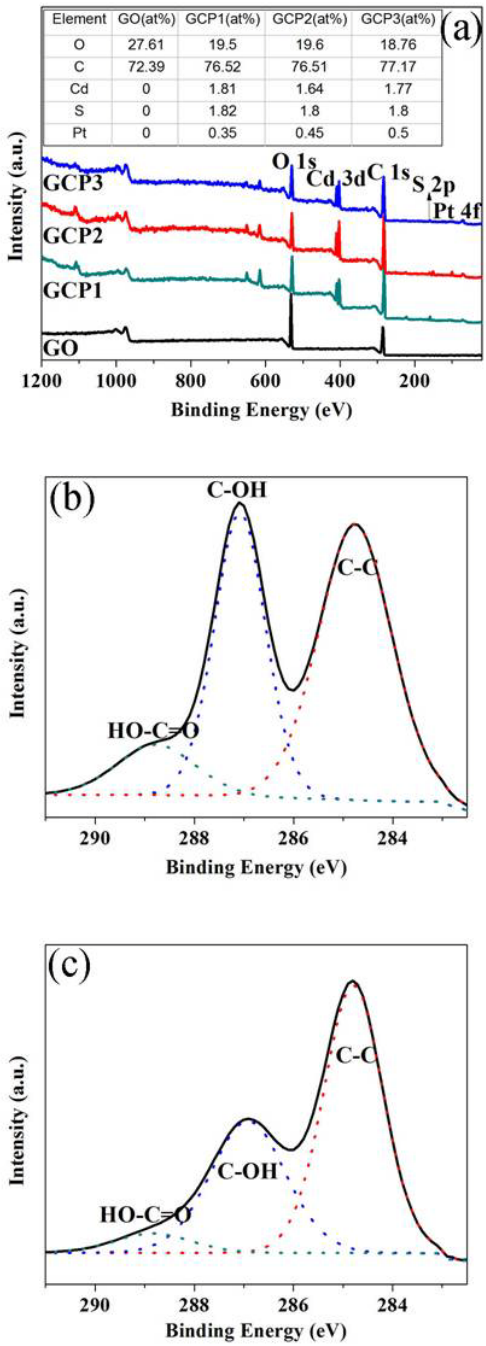

Fig. 4 Full XPS spectra of GO, GCP-1, GCP-2 and GCP-3 (a); high-resolution XPS spectrum of C 1s from GO (b); and high-resolution XPS spectra of C 1s (c) from GCP-3, respectively.

later. In addition, the average O/C atomic ratio of all GO-CdS-Pt samples is 0.25 and the ratio is smaller than 0.38 of pure GO. The decrease of O/C atomic ratio further confirms the partial reduction of GO sheets, which is also reported in our previous reports.[24, 30] The evident decrease in oxygen content is also confirmed by high-resolution XPS spectra of C 1s from GO and GCP-3 in Fig. 4 (b) and (c). As shown in Fig. 4 (b) and (c), in comparison with GO, both epoxy/hydroxyl (C-OH, 286.9 eV) and carboxyl (HO-C=O, 288.9 eV)[15, 26, 30] attributing to the oxygen-containing functional groups are decreased obviously, indicating the effectively partial reduction of GO by formic acid. Therefore, GO-CdS-Pt nanocomposites can be dissolved in water very well with improved charge transfer ability. Fig. S3† (a), (b) and (c) show the high-resolution XPS spectra of Cd 3d, S 2p and Pt 4f from GCP-3, individually, which coordinate well with that of typical spectra from the reported literatures.[8, 30, 34] The results analyzed from XPS spectra are in consistent with results of FT-IR, indicating CdS and Pt nanoparticles are successfully deposited on partial reduced GO sheets.

Photocatalytic hydrogen evolution activity and mechanism

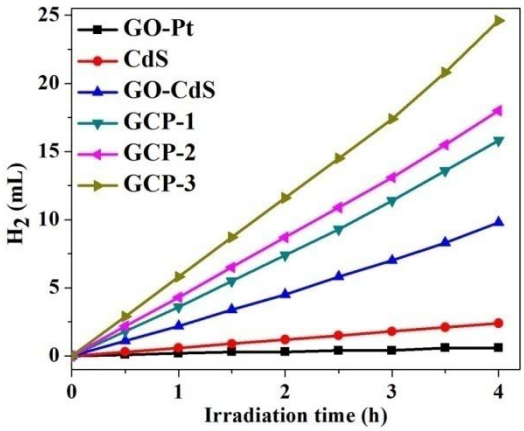

Fig. 5 Hydrogen evolution of GO-Pt, CdS, GO-CdS, GCP-1, GCP-2 and GCP-3 within 4 h, respectively.

Photocatalytic hydrogen evolution activities of prepared samples were evaluated under a 400 W high pressure Hg lamp (peak wavelength ca. 365 nm) using methanol as a sacrificial reagent. Fig. 5 shows the amount of hydrogen generated within 4 h by 50 mg of GO-Pt, CdS, GO-CdS, GCP-1, GCP-2 and GCP-3, respectively. GO-Pt shows almost no hydrogen produced during 4 h because GO-Pt cannot absorb light, which has been confirmed by previous report.[15] In addition, it can be clearly seen that GO and Pt exhibit important influence on the photocatalytic ability. In Fig. 5, pure CdS nanoparticles generate only 2.4 mL H_2 within 4 h. Such low evolution activity is due to the rapid recombination of photogenerated electron-hole pairs of CdS. However, GO-CdS shows much higher hydrogen evolution activity than CdS and 9.8 mL H_2 is produced during photocatalytic process. This is because GO serves as an acceptor of photogenerated electrons from CdS to reduce the recombination probability of electron-hole pairs.[24] When combining GO-CdS with different amounts of Pt nanoparticles, the hydrogen evolution efficiency is further enhanced. GCP-1, GCP-2 and GCP-3 generate 15.8 mL, 18 mL and 24.6 mL H_2 within 4 h, individually, which is much higher than that of CdS and GO-CdS. Fig. 6 (a) exhibits average H_2-evolution rates of GO-Pt, CdS, GO-CdS, GCP-1, GCP-2 and GCP-3 in 4 h reactions, individually. In this work, GCP-3 displays the highest H_2-evolution rate of 123 mL $h^{-1}g^{-1}$, which is about 10.3 times higher than that of CdS, and 2.5 times higher than that of GO-CdS.

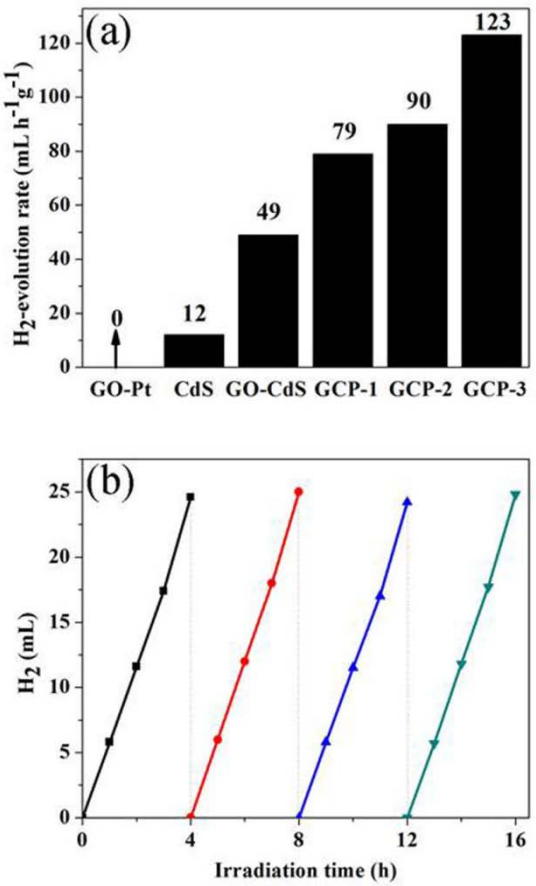

Fig. 6 Average hydrogen evolution rates in 4 h reactions (a) and recycling test of hydrogen evolution of GCP-3 (b).

In addition, this H_2-evolution rate—123 mL $h^{-1}g^{-1}$ (5500 μmol $h^{-1}g^{-1}$) is much higher than that of GO-TiO_2 composites (736 μmol $h^{-1}g^{-1}$)[35] and N-Graphene/CdS (1050 μmol $h^{-1}g^{-1}$).[19] Furthermore, the photostability of GCP-3 is investigated. As shown in Fig. 6 (b), photocatalytic hydrogen evolution activity remains almost at the same level in four cycles, indicating GCP-3 is very photostable. High hydrogen evolution efficiency and strong durability of GO-CdS-Pt nanocomposites can be explained by Fig. 7.

In GO-CdS-Pt system, firstly, CdS can be excited by UV light to generate electrons and holes. Then the photogenerated electrons transfer to GO while holes are leaved behind in CdS since the conduction band of CdS is more negative. This electron transfer route reduces the possibility of recombination of electron-hole pairs and prolongs the lifetime of charge carriers. In addition, GO in GO-CdS-Pt composites is partially reduced from the analysis of FT-IR and XPS spectra. According to the mechanism of Hoffman et al.,[36] the higher conductivity leads to more efficient charge transfer and anti-recombination, so the H_2-evolution rates of GO-CdS-Pt nanocomposites are faster than that of GO-CdS and CdS. Furthermore, the work function of GO is about 4.42 eV,[37, 38] while that of Pt is 5.64 eV,[23] so the photogenerated electrons transfer from GO to Pt is energetically favorable.[23, 38] As a consequence, the vectorial electron transfer route of GO-CdS-Pt can be realized along CdS→GO→Pt, as

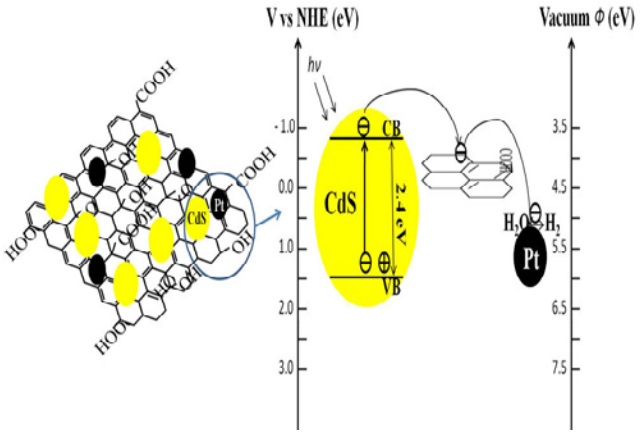

Fig. 7 Schematic illustration of the charge separation and transfer in GO-CdS-Pt system.

shown in Fig. 7. Effective charge transfer and anti-recombination leads to high hydrogen evolution efficiency and strong photostability. Furthermore, the ability of light absorption for these GO-CdS-Pt nanocomposites is nearly equal because CdS amount in GCP-1, GCP-2 and GCP-3 is almost the same based on the analysis of XPS. However, the atomic ratio of Pt for GCP-1, GCP-2 and GCP-3 is rising, resulting in an increased H_2-evolution rate, because more Pt nanoparticles supply more reactive sites for hydrogen production. Consequently, GCP-3 with 0.5 at% of Pt exhibits the highest H_2-evolution rate of 123 mL $h^{-1}g^{-1}$. In addition, it is interesting to find that the H_2-generation rate is slightly increased during the later period (3-4 h) of photocatalytic process than early period (1-3 h). This phenomenon can be attributed to the further reduction of GO by photogenerated electrons during the hydrogen evolution process, which is confirmed by the high resolution XPS spectrum of C 1s from GCP-3 after hydrogen generation process, as shown in Fig. S4†. The conductivity increases in the later period, leading to higher H_2-evolution rate.

Conclusions

In summary, highly efficient GO-CdS-Pt nanocomposites for hydrogen evolution are successfully prepared through combining formic acid reduction process with two-phase mixing method. The morphology and structure of these composites are extensively investigated by AFM, TEM, XRD, FT-IR and XPS spectroscopy, confirming the well deposition of CdS and Pt nanoparticles on GO sheets. In addition, the hydrogen evolution efficiency of GO-CdS-Pt nanocomposites with different amounts of Pt is discussed. The highest hydrogen production rate achieved by GO-CdS-Pt nanocomposite containing 0.5 at% of Pt is 123 mL $h^{-1}g^{-1}$ in our work, which is much higher than that of pure CdS and GO-CdS. Furthermore, GO-CdS-Pt is photostable during the hydrogen evolution process within 16 h. These results indicate that both GO and Pt play significant roles in achieving high hydrogen evolution efficiency and inhibited photocorrosion. Partial reduced GO with improved conductivity acts as electron acceptor to reduce the recombination probability of photogenerated electron-hole pairs. In addition, suitably positioned work functions of respective component, including CdS, GO and Pt of GO-CdS-Pt composites, facilitate vectorial

charge transfer. This work highlights the potential applications of GO-CdS-Pt composites in green energy production field.

Acknowledgements

Authors would like to acknowledge the Clean Energy Research Programme under National Research Foundation of Singapore for their research grant (Grant No. NRF2007EWT-CERP01-0420) support for this work.

Notes and references

School of Civil and Environmental Engineering, Nanyang Technological University, Singapore 639798.
Email: JCLIU@ntu.edu.sg; DDSUN@ntu.edu.sg; Fax: +65 6791-0676; Tel: +65 6790-6273
† Electronic Supplementary Information (ESI) available: More AFM, TEM images and XPS spectra. See DOI: 10.1039/b000000x/

1. R. M. Dell and D. A. J. Rand, *J. Power Sources*, 2001, **100**, 2-17.
2. E. Chornet and S. Czernik, *Nature*, 2002, **418**, 928-929.
3. R. D. Cortright, R. R. Davda and J. A. Dumesic, *Nature*, 2002, **418**, 964-967.
4. R. M. Navarro, M. A. Peña and J. L. G. Fierro, *Chem. Rev.*, 2007, **107**, 3952-3991.
5. J. Ng, S. Xu, X. Zhang, H. Y. Yang and D. D. Sun, *Adv. Funct. Mater.*, 2010, **20**, 4287-4294.
6. A. Fujishima and K. Honda, *Nature*, 1972, **238**, 37-38.
7. S. Xu, J. Ng, A. J. Du, J. Liu and D. D. Sun, *Int. J. Hydrogen Energy*, 2011, **36**, 6538-6545.
8. S. K. Apte, S. N. Garaje, G. P. Mane, A. Vinu, S. D. Naik, D. P. Amalnerkar and B. B. Kale, *Small*, 2011, **7**, 957-964.
9. K. Sivula, F. L. Formal and M. Grätzel, *Chem. Mater.*, 2009, **21**, 2862-2867.
10. S. Xu, A. J. Du, J. Liu, J. Ng and D. D. Sun, *Int. J. Hydrogen Energy*, 2011, **36**, 6560-6568.
11. K. Wegner, H. C. Ly, R. J. Weiss, S. E. Pratsinis and A. Steinfeld, *Int. J. Hydrogen Energy*, 2006, **31**, 55-61.
12. Y. Li, J. Wang, S. Peng, G. Lu and S. Li, *Int. J. Hydrogen Energy*, 2010, **35**, 7116-7126.
13. Y. X. Li, Y. F. Hu, S. Q. Peng, G. X. Lu and S. B. Li, *J. Phys. Chem. C*, 2009, **113**, 9352-9358.
14. X. B. Chen, S. H. Shen, L. J. Guo and S. S. Mao, *Chem. Rev.*, 2010, **110**, 6503-6570.
15. Q. Li, B. Guo, J. Yu, J. Ran, B. Zhang, H. Yan and J. R. Gong, *J. Am. Chem. Soc.*, 2011, **133**, 10878-10884.
16. G. S. Li, D. Q. Zhang and J. C. Yu, *Environ. Sci. Technol.*, 2009, **43**, 7079-7085.
17. G. Dukovic, M. G. Merkle, J. H. Nelson, S. M. Hughes and A. P. Alivisatos, *Adv. Mater.*, 2008, **20**, 4306-4311.
18. A. Cao, Z. Liu, S. Chu, M. Wu, Z. Ye, Z. Cai, Y. Chang, S. Wang, Q. Gong and Y. Liu, *Adv. Mater.*, 2010, **22**, 103-106.
19. L. Jia, D. H. Wang, Y. X. Huang, A. W. Xu and H. Q. Yu, *J. Phys. Chem. C*, 2011, **115**, 11466-11473.
20. S. Stankovich, D. A. Dikin, G. H. B. Dommett, K. M. Kohlhaas, E. J. Zimney, E. A. Stach, R. D. Piner, S. T. Nguyen and R. S. Ruoff, *Nature*, 2006, **442**, 282-286.
21. D. A. Dikin, S. Stankovich, E. J. Zimney, R. D. Piner, G. H. B. Dommett, G. Evmenenko, S. T. Nguyen and R. S. Ruoff, *Nature*, 2007, **448**, 457-460.
22. S. Guo and S. Dong, *Chem. Soc. Rev.*, 2011, **40**, 2644-2672.
23. Y. K. Kim and H. Park, *Energy Environ. Sci.*, 2011, **4**, 685.
24. J. Liu, H. Bai, Y. Wang, Z. Liu, X. Zhang and D. D. Sun, *Adv. Funct. Mater.*, 2010, **20**, 4175-4181.
25. W. S. Hummers and R. E. Offeman, *J. Am. Chem. Soc.*, 1958, **80**, 1339-1339.
26. J. Liu, H. Jeong, K. Lee, J. Y. Park, Y. H. Ahn and S. Lee, *Carbon*, 2010, **48**, 2282-2289.
27. J. Joo, H. B. Na, T. Yu, J. H. Yu, Y. W. Kim, F. Wu, J. Z. Zhang and T. Hyeon, *J. Am. Chem. Soc.*, 2003, **125**, 11100-11105.
28. J. Liu, L. Liu, H. Bai, Y. Wang and D. D. Sun, *Appl. Catal., B* 2011.
29. C. Chen, W. Cai, M. Long, B. Zhou, Y. Wu, D. Wu and Y. Feng, *ACS Nano*, 2010, **4**, 6425-6432.
30. Y. J. Wang, J. C. Liu, L. Liu and D. D. Sun, *Nanoscale Research Letters*, 2011, **6**.
31. W. W. Yu, L. H. Qu, W. Z. Guo and X. G. Peng, *Chem. Mater.*, 2003, **15**, 2854-2860.
32. Y. Xu, H. Bai, G. Lu, C. Li and G. Shi, *J. Am. Chem. Soc.*, 2008, **130**, 5856-5857.
33. G. I. Titelman, V. Gelman, S. Bron, R. L. Khalfin, Y. Cohen and H. Bianco-Peled, *Carbon*, 2005, **43**, 641-649.
34. K. Zhang and X. Liu, *Appl. Surf. Sci.*, 2011, **257**, 10379-10383.
35. Q. Xiang, J. Yu and M. Jaroniec, *Nanoscale*, 2011, **3**, 3670-3678.
36. M. R. Hoffmann, S. T. Martin, W. Choi and D. W. Bahnemann, *Chem. Rev.*, 1995, **95**, 69-96.
37. R. Czerw, B. Foley, D. Tekleab, A. Rubio, P. M. Ajayan and D. L. Carroll, *Physical Review B*, 2002, **66**.
38. C. X. Guo, H. B. Yang, Z. M. Sheng, Z. S. Lu, Q. L. Song and C. M. Li, *Angew. Chem. Int. Ed.*, 2010, **49**, 3014-3017.